Available online at www.sciencedirect.com
SCIENCE DIRECT®
Biochemical and Biophysical Research Communications 332 (2005) 17–27
BBRC
www.elsevier.com/locate/ybbrc

# Identification and characterization of splice variants of the human $P2X_7$ ATP channel

Boonlert Cheewatrakoolpong [a], Helen Gilchrest [a], John C. Anthes [b], Scott Greenfeder [a,*]

[a] Department of Cardiovascular/Metabolism, Schering-Plough Research Institute, 2015 Galloping Hill Road, Kenilworth, NJ 07033, USA
[b] Department of Neurobiology, Schering-Plough Research Institute, 2015 Galloping Hill Road, Kenilworth, NJ 07033, USA

Received 19 April 2005
Available online 26 April 2005

**Abstract**

The P2X7 channel is a member of the P2X family of ligand-gated ion channels which respond to ATP as the endogenous agonist. Studies suggest that P2X7 has a potentially pivotal role in inflammatory responses largely stemming from its role in mediating the release of IL-1β in response to ATP. We report the identification of seven variants of human P2X7 which result from alternative splicing. Two of these variants (one lacking the first transmembrane domain, the second lacking the entire cytoplasmic tail) were compared to the full-length channel. Real-time PCR analysis demonstrated that both variants were expressed in various tissues and that the cytoplasmic tail deleted variant is highly expressed. Deletion of the first transmembrane domain resulted in a non-functional channel. Deletion of the cytoplasmic tail did not affect ion movement but severely affected the ability to form a large pore and to induce activation of caspases.


*Keywords:* Purinoreceptor; $P2X_7$; Bz-ATP; Ox-ATP

The $P2X_7$ channel is a member of the P2X family of ligand-gated ion channels. These channels respond to ATP as the endogenous ligand and differ in distribution, gating properties, and affinity for ATP and different ATP analogs [1,2]. All of the P2Xs respond to activation with movement of cations both into and out of the cell. $P2X_7$ is unique among the family in that continued stimulation results in the formation of a larger pore which facilitates the uptake of cationic molecules up to 900 D [1,3]. In addition, $P2X_7$ has a much larger carboxy terminus than other members of the P2X family which may be responsible for the additional functions of $P2X_7$ [4]. Further activation of $P2X_7$ in some cell types results in the induction of apoptosis [1,3,5,6].

$P2X_7$ is expressed primarily on cells of hematopoietic lineage including monocytes, macrophages, microglia, dendritic cells, T-cells, and B-cells [1]. The best characterized activity of $P2X_7$ is its role in ATP-induced IL-1β release from macrophages and microglia that have been primed with substances such as bacterial endotoxin [7–11]. Additionally, $P2X_7$ has been shown to play an important role in ATP-mediated killing of intracellular pathogens in macrophages [12,13]. Hence, $P2X_7$ is considered to have a potentially pivotal role in various inflammatory conditions.

It has been shown that the ATP-induced increase in IL-1β release is mediated through the activation of IL-1 converting enzyme, or ICE, a member of the caspase family of proteases [14,15]. It is largely held that activation of $P2X_7$ triggers the efflux of $K^+$ from cells which in turn activates ICE. ICE then cleaves pro-IL-1β to mature IL-1β facilitating its release from the cell. Less well characterized, but no less important, $P2X_7$ has also been

* Corresponding author.
*E-mail address:* scott.greenfeder@spcorp.com (S. Greenfeder).

0006-291X/$ - see front matter © 2005 Elsevier Inc. All rights reserved.
doi:10.1016/j.bbrc.2005.04.087

shown to play roles in the function of T-cells, dendritic cells, osteoblasts, osteoclasts, B-cells, eosinophils, smooth muscle cells, and fibroblasts [1].

Direct evidence for an important physiological role for the channel comes from recent studies of mice deficient in $P2X_7$. Deletion of $P2X_7$ abolishes the ability of extracellular ATP to induce IL-1β release from isolated macrophages [16]. Further analyses of these mice reveal that $P2X_7$ may play an important role in immune-based diseases such as rheumatoid arthritis. $P2X_7$ deficient mice are protected against symptom development and cartilage destruction in anti-collagen antibody-induced arthritis [17]. It is also of interest to note that the ability of $P2X_7$ deficient mice to raise an antibody response was not affected.

In the present study, we have identified splice variants of the human $P2X_7$ channel. Two of these variants were characterized for expression and function. Our results demonstrate that a splice variant lacking the carboxy terminus is highly expressed in many tissues and maintains the ability to respond to ATP with cation movement but is deficient in pore formation as measured by ethidium bromide (EtBr) uptake.

## Materials and methods

*Reagents.* ATP and benzoyl-benzoyl-ATP (Bz-ATP) and other chemicals were purchased from Sigma–Aldrich (St. Louis, MO). All tissue culture reagents were purchased from Invitrogen (Carlsbad, CA).

*Cloning and identification of $P2X_7$ splice variants.* A coding sequence of human $P2X_7$ (GenBank Accession No. Y09561) was cloned by a polymerase chain reaction (PCR). A marathon-ready human brain cDNA (BD Biosciences, Palo Alto, CA) was used as a template. In some cases, cDNAs prepared from total RNA of THP-1 cells (American Type Culture Collection, Rockville, MD), liver (BD Biosciences), and peripheral blood mononuclear cells (PBMC, BD Biosciences) were also used. The forward primer (with *Hin*dIII site) used was 5′ CTTAAGCTTACCATGCCGGCCTGCTGCAGCTG 3′ and the reverse primer (with *Xba*I site) was 5′ TCTCTAGATCAGTAAG GACTCTTGAAGCCAC 3′. The PCRs were carried out using ExTaq polymerase (with 3′ proofreading and exonuclease activities) (Invitrogen, Carlsbad, CA) for 30 cycles with the temperature cyclings as follows: denaturation at 94 °C for 30 s, annealing at 60 °C for 30 s, and extension for 2 min, followed by a final extension for 7 min at 68 °C. All PCR products were purified, digested with *Hin*dIII and *Xba*I enzymes, and cloned into a *Hin*dIII/*Xba*I digested pcDNA3.1 (+) vector (Invitrogen, Carlsbad, CA). Plasmids from different clones were prepared and the sequence of each insert was verified by double-stranded sequencing (Sequetech, Mountain View, CA).

Variants were subsequently sub-cloned by PCR using primers specific to each variant. For the variant lacking TM1 (Δ-TMI) the forward primer (with *Hin*dIII site) was 5′ CTTAAGCTTA CCATGA CTCCAG GAGACCATTC 3′. The reverse primer was the same as that for the cloning of the full-length $P2X_7$ (above). For the variant with a truncated C-terminus (Δ-C) the forward primer was the same as that for the full-length $P2X_7$, and the reverse primer (with *Xba*I site) was 5′ TCTCTAGATTAGTCACTTCCTTCTCCAAACC 3′. The PCR products were cloned into pcDNA3.1(+) and sequenced as described above.

*Construction of N-terminal-tagged $P2X_7$.* To confirm the levels of expression of different $P2X_7$ variants in HEK-293 cells, $P2X_7$ constructs were generated by PCR and cloned into pTriEx-4Neo (Novagen, San Diego, CA). $P2X_7$ expressed from these constructs contained S-tag protein in their N-termini. The forward primer for cloning the full-length and Δ-C $P2X_7$ (with *Not*I site) was 5′ CTTGCGGCCGC AATGCCGGCCTGCTGCAGCTG 3′, and that for Δ-TMI (with *Not*I site) was 5′ CTTGCGGCCGCAATGACTCCAGGAGACC ATTC 3′. The reverse primer for both the full-length and Δ-TMI $P2X_7$ (with *Xho*I site) was 5′ GTGCTCGAGA TCTTAGTAAGGACTC TTGAA 3′. For Δ-C, the reverse primer (with *Xho*I site) used in the PCR was 5′GTGCTCGAGATCTTTTAGTCACTT CCTTCTC 3′.

*Real-time PCR analysis.* cDNAs from various cell types and tissues were obtained from BD Biosciences. The expression profile of $P2X_7$ variants was carried out by a real-time quantitative PCR method using a SYBR Green kit (Applied Biosystems, Foster City, CA) on an ABI Prism 7700 Sequence Detection System (Applied Biosystems). The $P2X_7$ variant-specific forward and reverse primer sets were as follows: Δ-TMI (forward: 5′ CAAGGTCAGCCGAGATTCAG 3′; reverse: 5′ CCGAAGTAGGAGAGGGTTGAG 3′); Δ-C (forward: 5′ CGGCCA CAACTACACCACGAG 3′; reverse: 5′ CAGGGCTGACAGCACT TGCAC 3′). The generic primers that detect the common region of all variants were 5′ GAACCAGCAGCTACTAGGGAGAAG 3′ (forward) and 5′ TGGGCAGGTTGGCAAAGTCAGC 3′ (reverse), respectively. For G3PDH, the forward primer was 5′ CCTCTGACTT CAACAGCGAC 3′ and the reverse primer was 5′ CATGACAAGGT GCGGCTCCC 3′. A standard curve for each $P2X_7$ variant was constructed using a corresponding plasmid DNA as a template. For G3PDH, a standard curve was created using a PCR fragment amplified with the primer pair described above.

*Western blotting.* Whole cell lysate was prepared from approximately $10 \times 10^6$ cells stably expressing each S-tagged $P2X_7$ variant. Cell pellet was sonicated in 1 ml ice-cold lysis buffer (20 mM Tris–HCl, pH 8.0, containing 1% Nonidet P-40, 150 mM NaCl, 1 mM EDTA, 1 mM sodium orthovanadate, 5 mM sodium fluoride, and 5 mM sodium pyrophosphate) supplemented with a protease inhibitor cocktail (Roche Applied science, Indianapolis, IN). The lysate was centrifuged for 10 min at 10,000*g* at 4 °C, and the supernatant (50 μg protein/sample) was used for reduced SDS–PAGE and subsequent Western blot. S-protein-HRP (Novagen) was used for the detection of S-tagged $P2X_7$ followed by a chemiluminescence signal development using a West Pico kit (Pierce, New York, NY).

*EtBr uptake analysis.* Ethidium bromide (EtBr) uptake was carried out as previously described with some modifications [18]. Briefly, HEK-293 cells stably expressing $P2X_7$ were harvested and seeded into a black-poly-D-lysine-coated 96-well plate (40,000 cells/well in 200 μl culture medium) 24 h prior to assay. Before the assay, culture medium was replaced with 100 μl of dye uptake buffer (280 mM sucrose, 5 mM KCl, 0.5 mM $CaCl_2$, 10 mM glucose, 10 mM Hepes, and 10 mM *N*-methyl-D-glucamine, pH 7.4) containing 50 μM EtBr. Cells were subsequently treated with different concentrations of Bz-ATP (100 μl/well) prepared in dye uptake-EtBr buffer. The EtBr uptake was monitored for 10 min using a FLEXstation imaging plate reader (Molecular Devices, Sunnyvale, CA) with an excitation wavelength of 525 nm and emission wavelength of 610 nm. Cells were pretreated with various concentrations of antagonists for 30 min at 37 °C before the addition of Bz-ATP (200 μM).

*Apoptosis measurements.* For apoptosis studies, cells were set up in the same manner as that for the EtBr uptake studies. ApoONE reagent (Promega, Madison, WI) was used to measure the caspase 3 and 7 activities induced by $P2X_7$ agonists. The M30-apoptosense ELISA (DiaPharma Grp., Columbus, OH) was used to follow the cleavage of cytokeratin-18.

*Determination of $Ca^{2+}$ uptake and membrane potential changes.* HEK-293 cells stably expressing various $P2X_7$ variants were plated into poly-D-lysine-coated Biocoat 96-well clear-bottom black plates (BD Biosciences, Bedford, MA) at 40,000–70,000 cells/well in 200 μl of

growth medium and grown for 24–48 h. Medium was removed and cells were incubated for 1 h at 37 °C in 180 μl loading buffer (145 mM NaCl, 2 mM KCl, 0.3 mM $CaCl_2$, 10 mM Hepes, 10 mM D-glucose, and 2.5 mM probenecid containing 1× Calcium Plus no-wash dye (Molecular Devices, Sunnyvale, CA)). Plates were transferred to a Fluorometric Imaging Plate Reader (FLIPR) (Molecular Devices, Sunnyvale, CA) heated to 37 °C. Responses were elicited by the addition of 20 μl of 10× agonist (Bz-ATP) solution and the fluorescent signal was monitored for 2 min Antagonists, when assayed, were included during the dye loading step. The fluorescent signal was quantitated as the total area under the response curve over the 2 min run time. Reported data are normalized to the response to 10 μM ionophore (A23187).

Membrane potential was measured in a FLIPR. Loading buffer used was as mentioned above with 0.5× Membrane Potential Dye (Molecular Devices, Sunnyvale, CA). Dye loading was carried out for 30–45 min at room temperature. Plates were transferred to a FLIPR heated to 37 °C and allowed to equilibrate for at least 10 min. The fluorescent signal was quantitated in the same manner as above. Reported data are normalized to the response to 7.5 mM KCl.

## Results

### *Isolation and structure of splice variants*

While cloning the human $P2X_7$ cDNA eight different variants were identified that apparently result from alternative splicing events. It is highly unlikely that these variants are artifacts resulting from the PCR cloning method used since the polymerase employed has proofreading and exonuclease activities. Furthermore, each of the variants identified occurs precisely on known or putative splice donor/acceptor pairs.

The human $P2X_7$ gene was originally described as containing 13 exons as shown in Fig. 1A [19]. These 13 exons encode a 595 amino acid protein consisting of two transmembrane domains, intracellular amino- and carboxy termini and a large extracellular loop. The $P2X_7$A variant shown in Fig. 1B is the previously identified full-length cDNA. The alignment of $P2X_7$ variant sequences with genomic DNA sequence (GenBank Accession No. NT-009775) revealed a new exon, tentatively termed N3, which is located in the intronic region between exons 2 and 3. Exon N3 is included in variants G and H (Fig. 1B). The sequence of exon N3 is shown in Fig. 2A. The inclusion of this exon creates a new start codon which potentially leads to the translation of a $P2X_7$ protein which lacks transmembrane domain I (TMI). Variants were also identified in which either exon 5, 7, 8 or 7 and 8 together were removed from the final cDNA (variants D, E, and F Fig. 1B). A third variation was the inclusion of the intron between exons 10 and 11 into the final cDNA due to the failure to appropriately excise this intron (variants B, E, and G). The inclusion of this intron introduces a new stop codon resulting in a shortened protein which lacks the last 171 amino acids of the full-length protein and alters the 18 amino acids following transmembrane domain II (Figs. 1B, variant B and 2). The sequence of this intron is shown in Fig. 2B. The alignment of the protein sequences of variants

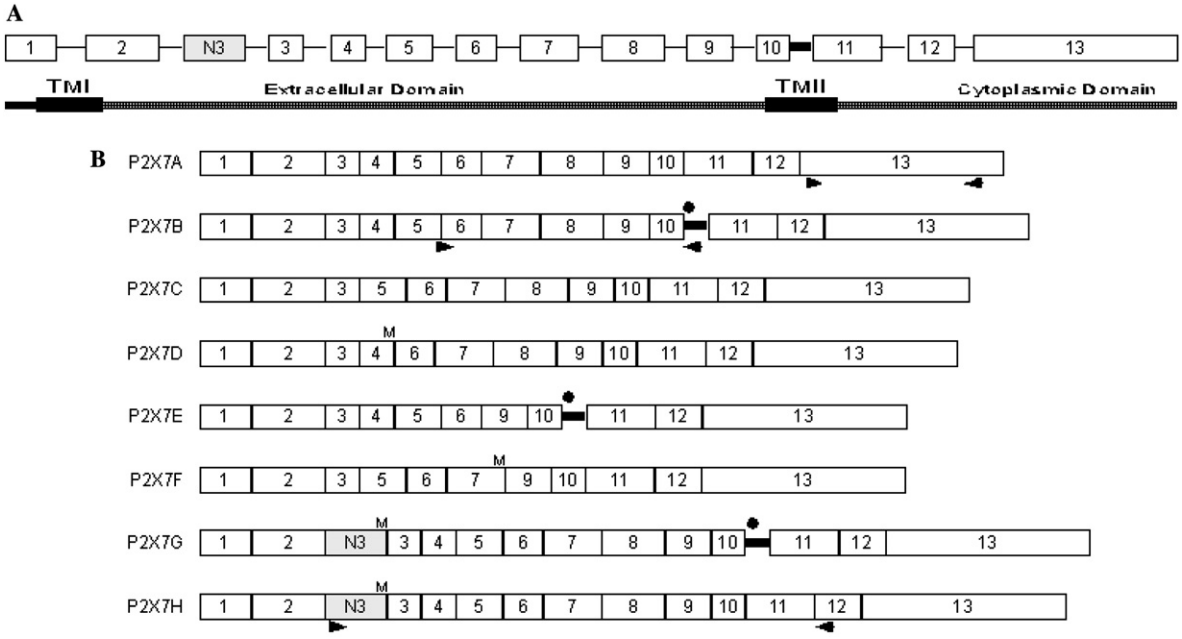


Fig. 1. (A) Genomic structure of the human $P2X_7$ gene is shown. Exons are numbered and indicated by boxes. The newly identified exon N3 is indicated. Introns are represented by horizontal lines between the exons. Below the genomic structure is depicted the $P2X_7$ transcript with relevant domains indicated. (B) The exon arrangement of the various splice variants isolated is shown. New stop codons are indicated by asterisks and new start codons indicated by the letter M. The approximate positions of PCR primers used for real-time expression analysis are indicated by arrowheads placed below variants A, B, and H. The sequences of the seven splice variants have been deposited in GenBank with the following Accession Nos. AY847298, AY847299, AY847300, AY847301, AY847302, AY847303, and AY847304.

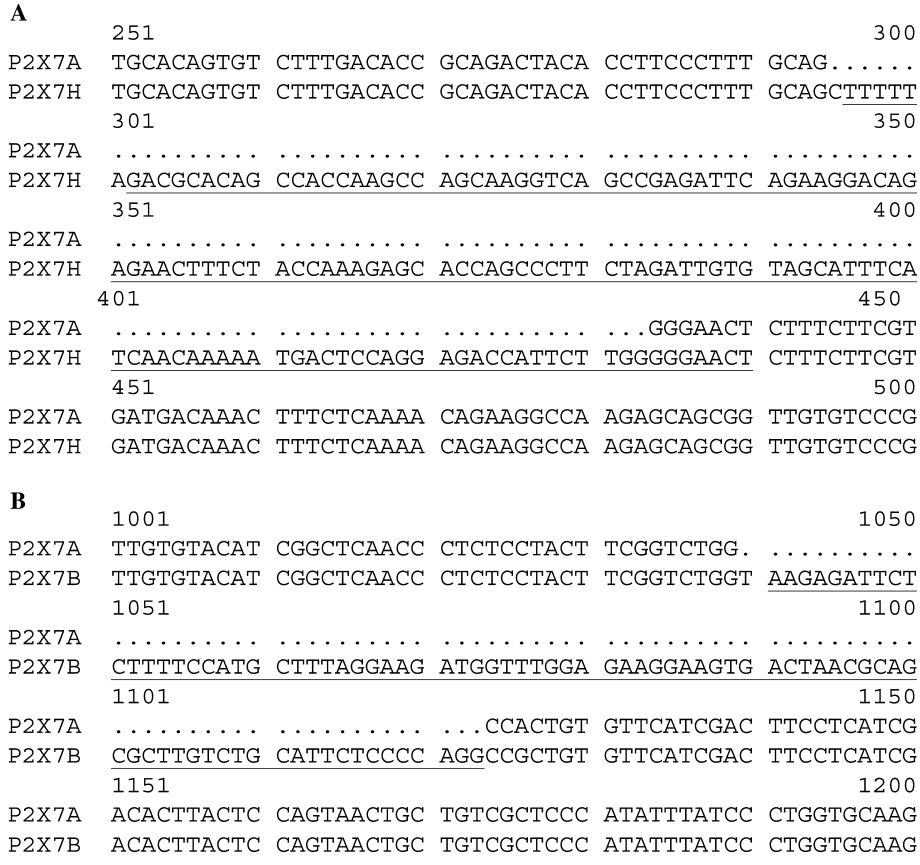


Fig. 2. (A) The nucleotide alignment of $P2X_7A$ (full-length) and $P2X_7H$ (Δ-TMI) is shown in the region of insertion of exon N3. The exon N3 sequence is underlined. (B) The nucleotide alignment of $P2X_7A$ (full-length) and $P2X_7B$ (Δ-C) is shown in the region of the retention of the intron between exons 10 and 11. The retained intronic sequence is underlined.

A, B, and H is shown in Fig. 3. Variant A is the full-length $P2X_7$, B, the C-terminus deleted (Δ-C), and H, the TMI deleted (Δ-TMI) variant. The Δ-C and Δ-TMI variants were chosen for further evaluation of expression and function since these were the variants for which we could develop specific reagents to analyze gene expression. Attempts to develop similar reagents for the other identified variants were unsuccessful.

*Splice variant expression pattern*

Primers were designed, as described in Materials and methods, that detected either all forms of human $P2X_7$, or specifically the Δ-TMI variant or specifically the Δ-C variant. The specificity of these primer pairs was verified using the cloned cDNA for each form as well as brain and THP-1 cDNAs. A single band of PCR product with the expected sequence was always obtained with each set of primers (data not shown). Real-time SYBR-green PCR was carried out using each of the cloned cDNAs to generate standard curves. Expression levels for total $P2X_7$, Δ-TMI, and Δ-C were determined and are expressed in Fig. 4 as fg of $P2X_7$/pg G3PDH.

Fig. 4A shows the expression of the various forms in a collection of human tissues and Fig. 4B shows the expression in resting or activated total peripheral blood mononuclear cells (PBMC), T-cells ($CD4^+$ and $CD8^+$), B-cells ($CD19^+$), and resting monocyte/macrophages ($CD14^+$). Consistent with previous studies $P2X_7$ is widely expressed with highest levels in brain and immune tissues (Fig. 4A). In general, the expression of the Δ-TMI form is very low. Interestingly, in most samples tested the Δ-C form is the most abundantly expressed suggesting that this may be the predominant form of $P2X_7$. A notable exception is resting CD19 expressing cells (B-cells). In this case, the expression of the Δ-TMI and Δ-C variants is very low, indicating that the full length (or another variant) is the predominant form (Fig. 4B). Other samples in which there is significant expression of full-length $P2X_7$ include lymph node, brain, resting $CD4^+$ T-cells, and resting $CD14^+$ monocyte/macrophages. It is interesting to note that the expression of all variants is greatly reduced by activation of any of the cell types tested (Fig. 4B). We have corroborated the decrease in expression of $P2X_7$ in activated primary human T-cells and have also demonstrated a time-dependent

```
             1                                                   50
Full-length  MPACCSCSDV FQYETNKVTR IQSMNYGTIK WFFHVIIFSY VCFALVSDKL
    Delta-C  MPACCSCSDV FQYETNKVTR IQSMNYGTIK WFFHVIIFSY VCFALVSDKL
  Delta-TMI  .......... .......... .......... .......... ..........
             51                                                  100
Full-length  YQRKEPVISS VHTKVKGIAE VKEEIVENGV KKLVHSVFDT ADYTFPLQGN
    Delta-C  YQRKEPVISS VHTKVKGIAE VKEEIVENGV KKLVHSVFDT ADYTFPLQGN
  Delta-TMI  .......... .......... .......... .......... MTPGDHSWGN
             101                                                 150
Full-length  SFFVMTNFLK TEGQEQRLCP EYPTRRTLCS SDRGCKKGWM DPQSKGIQTG
    Delta-C  SFFVMTNFLK TEGQEQRLCP EYPTRRTLCS SDRGCKKGWM DPQSKGIQTG
  Delta-TMI  SFFVMTNFLK TEGQEQRLCP EYPTRRTLCS SDRGCKKGWM DPQSKGIQTG
             151                                                 200
Full-length  RCVVHEGNQK TCEVSAWCPI EAVEEAPRPA LLNSAENFTV LIKNNIDFPG
    Delta-C  RCVVHEGNQK TCEVSAWCPI EAVEEAPRPA LLNSAENFTV LIKNNIDFPG
  Delta-TMI  RCVVHEGNQK TCEVSAWCPI EAVEEAPRPA LLNSAENFTV LIKNNIDFPG
             201                                                 250
Full-length  HNYTTRNILP GLNITCTFHK TQNPQCPIFR LGDIFRETGD NFSDVAIQGG
    Delta-C  HNYTTRNILP GLNITCTFHK TQNPQCPIFR LGDIFRETGD NFSDVAIQGG
  Delta-TMI  HNYTTRNILP GLNITCTFHK TQNPQCPIFR LGDIFRETGD NFSDVAIQGG
             251                                                 300
Full-length  IMGIEIYWDC NLDRWFHHCH PKYSFRRLDD KTTNVSLYPG YNFRYAKYYK
    Delta-C  IMGIEIYWDC NLDRWFHHCH PKYSFRRLDD KTTNVSLYPG YNFRYAKYYK
  Delta-TMI  IMGIEIYWDC NLDRWFHHCH PKYSFRRLDD KTTNVSLYPG YNFRYAKYYK
             301                                                 350
Full-length  ENNVEKRTLI KVFGIRFDIL VFGTGGKFDI IQLVVYIGST LSYFGLAAVF
    Delta-C  ENNVEKRTLI KVFGIRFDIL VFGTGGKFDI IQLVVYIGST LSYFGLVRDS
  Delta-TMI  ENNVEKRTLI KVFGIRFDIL VFGTGGKFDI IQLVVYIGST LSYFGLAAVF
             351                                                 400
Full-length  IDFLIDTYSS NCCRSHIYPW CKCCQPCVVN EYYYRKKCES IVEPKPTLKY
    Delta-C  LFHALGRWFG EGSD...... .......... .......... ..........
  Delta-TMI  IDFLIDTYSS NCCRSHIYPW CKCCQPCVVN EYYYRKKCES IVEPKPTLKY
             401                                                 450
Full-length  VSFVDESHIR MVNQQLLGRS LQDVKGQEVP RPAMDFTDLS RLPLALHDTP
    Delta-C  .......... .......... .......... .......... ..........
  Delta-TMI  VSFVDESHIR MVNQQLLGRS LQDVKGQEVP RPAMDFTDLS RLPLALHDTP
             451                                                 500
Full-length  PIPGQPEEIQ LLRKEATPRS RDSPVWCQCG SCLPSQLPES HRCLEELCCR
    Delta-C  .......... .......... .......... .......... ..........
  Delta-TMI  PIPGQPEEIQ LLRKEATPRS RDSPVWCQCG SCLPSQLPES HRCLEELCCR
             501                                                 550
Full-length  KKPGACITTS ELFRKLVLSR HVLQFLLLYQ EPLLALDVDS TNSRLRHCAY
    Delta-C  .......... .......... .......... .......... ..........
  Delta-TMI  KKPGACITTS ELFRKLVLSR HVLQFLLLYQ EPLLALDVDS TNSRLRHCAY
             551                                                   596
Full-length  RCYATWRFGS QDMADFAILP SCCRWRIRKE FPKSEGQYSG FKSPY.
    Delta-C  .......... .......... .......... .......... ......
  Delta-TMI  RCYATWRFGS QDMADFAILP SCCRWRIRKE FPKSEGQYSG FKSPY.
```

Fig. 3. The amino acid sequences of the full-length, Δ-C, and Δ-TMI variants are aligned. The alignment was carried out using Vector NTI.

loss of $P2X_7$ function in these cells during activation (data not shown).

*Recombinant expression of $P2X_7$ variants*

Attempts to detect these proteins with commercially available antibodies directed against $P2X_7$ yielded unsatisfactory results limiting our ability to analyze the native form of these variants. In addition, all but one of the available antibodies are directed at the carboxy terminus of $P2X_7$ making them of no utility for analysis of the Δ-C variant. Therefore, in order to ascertain if the variant cDNAs could direct protein synthesis, stable HEK-293 cell lines were isolated expressing the full-length, Δ-C, and Δ-TMI variants of human $P2X_7$ each tagged with a S-tag epitope to facilitate identification. Lysates from these cells were subjected to Western blot analysis using S-protein-HRP. As shown in Fig. 5 full-length $P2X_7$ can be detected as a band of ~80 kDa. A band of ~70 kDa was detected in lysates from cells expressing the Δ-TMI variant and a band of ~53 kDa was detected in lysates from cells expressing the Δ-C variant. These sizes are consistent with those predicted from the amino acid sequences of each of

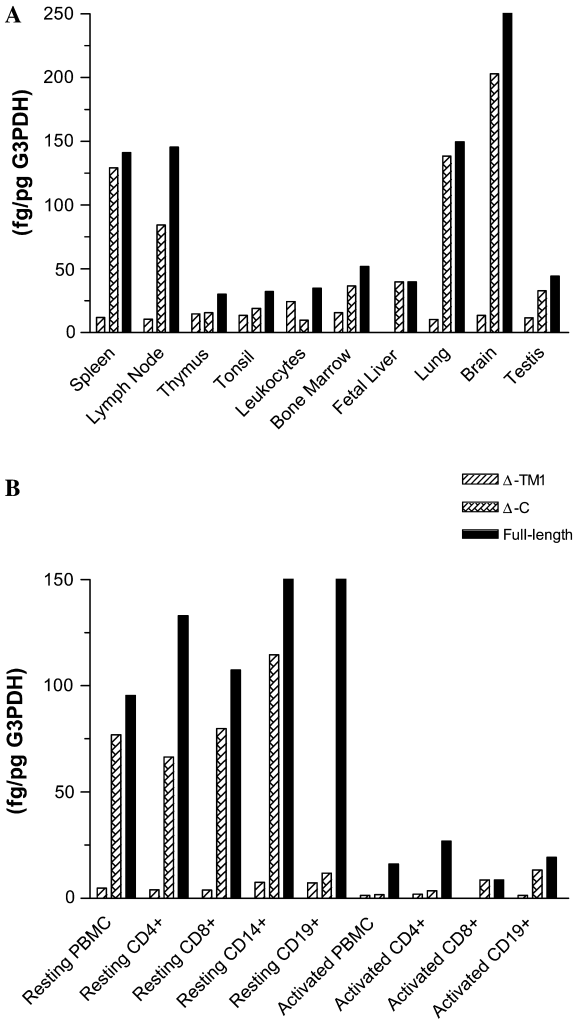


Fig. 4. Real-time PCR expression data are shown for all $P2X_7$ variants, Δ-C and Δ-TMI. Real-time PCR was carried out using the primers and as described in Materials and methods. Expression level is indicated as fg of $P2X_7$ variant transcript/pg of control transcript G3PDH.

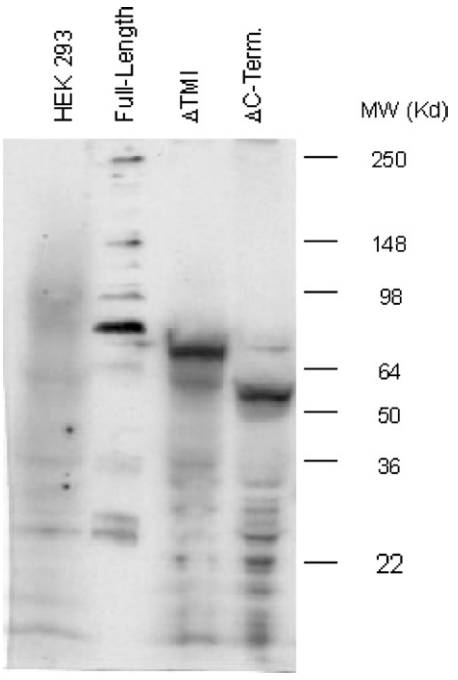


Fig. 5. Western blot analysis of lysates from cells recombinantly expressing $P2X_7$ variants is shown. Reducing SDS–PAGE was used to separate 50 μg/sample of protein prior to Western blotting.

the variants with the addition of ~10 kDa resulting from the tagging epitope. These data indicate that both the Δ-TMI and Δ-C cDNAs are capable of directing protein synthesis when expressed in HEK-293 cells.

### *Functional analysis of $P2X_7$ variants: $Ca^{2+}$ flux, membrane potential, and EtBr uptake*

Fluorescence-based assays demonstrate functional responses of both the full-length and Δ-C variants for either $Ca^{2+}$ flux (Fig. 6A) or membrane potential (Fig. 6B). The Δ-TMI variant did not respond to Bz-ATP in either $Ca^{2+}$ flux or membrane potential. Therefore, deletion of TM-1 renders $P2X_7$ inactive (data not shown). Bz-ATP causes a dose-dependent increase in intracellular calcium levels in both full-length and Δ-C variants with $EC_{50}$ values of 8 and 37 μM, respectively (Table 1, Fig. 6A). The Δ-C variant appears to be somewhat less sensitive to Bz-ATP as indicated by the rightward shift in the dose response. However, the efficacy of Bz-ATP is similar between the full-length and Δ-C variants with only a ~10% difference noted when compared to an ionophore control.

Bz-ATP was also tested in membrane potential assays. Bz-ATP causes a dose-dependent change in the fluorescent signal due to a hyperpolarization of the cellular membrane with $EC_{50}$s of 2 and 30 μM, respectively, for the full-length and Δ-C variants (Fig. 6B). Consistent with the $Ca^{2+}$ flux data, Bz-ATP is less potent at the Δ-C variant; however, the efficacy is similar for the two variants (Fig. 6B).

The full-length, Δ-C, and Δ-TMI variants were tested for the ability to facilitate the uptake of the large cationic dye EtBr. This function is indicative of the formation of a larger pore by $P2X_7$ [20]. Bz-ATP causes a dose-dependent increase in the uptake of EtBr in the full-length $P2X_7$ as measured by increased fluorescent signal. The Δ-C variant showed very little EtBr uptake in response to Bz-ATP (Fig. 6C). The Δ-TMI variant exhibited no Bz-ATP-induced EtBr uptake (data not shown). These data indicate that the Δ-C variant is unable to effectively adopt the larger pore structure that is formed by the full-length channel.

The $IC_{50}$ values for three $P2X_7$ antagonists were determined using both $Ca^{2+}$ flux and membrane potential assays. No differences in compound potencies were detected between assays. Ox-ATP has approximately

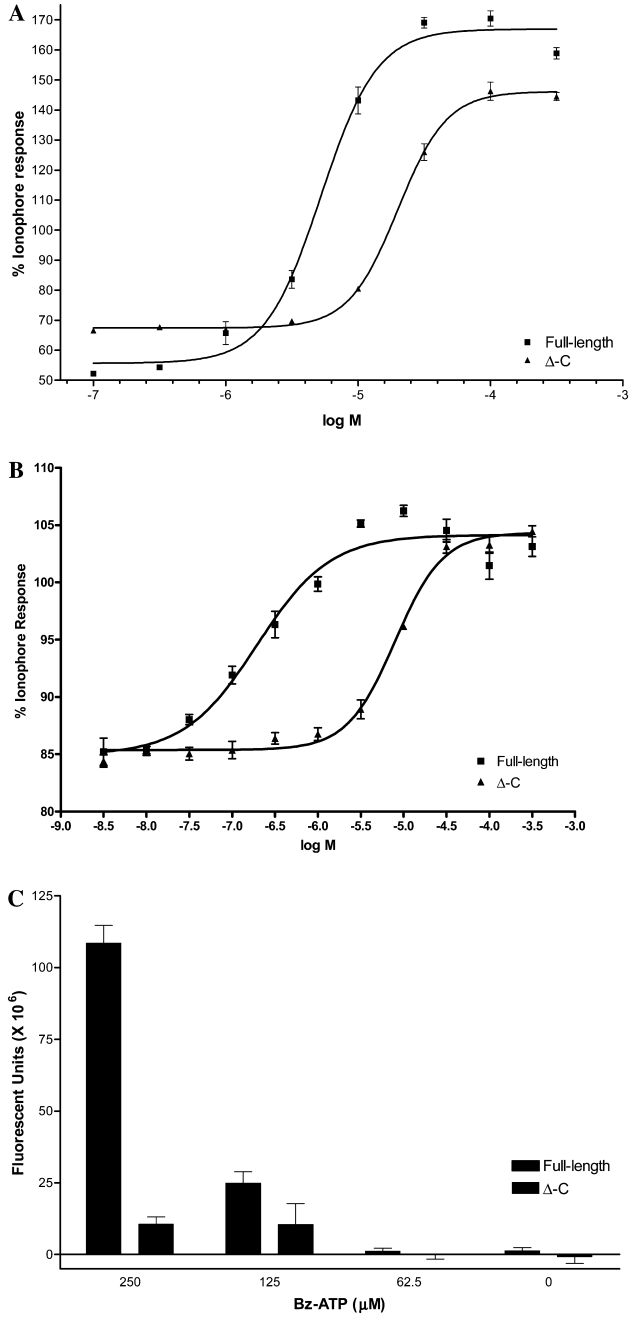


Fig. 6. Functional activity in cells stably expressing either the full-length or the Δ-C variant of $P2X_7$ is shown. (A) $Ca^{2+}$ flux elicited in cells by Bz-ATP is shown for full-length and Δ-C variants. The data are normalized to the total fluorescent response to 10 μM calcium ionophore and presented as the percent ionophore response. (B) Membrane potential changes elicited by Bz-ATP are shown for full-length and Δ-C variants. The data are normalized to the total fluorescent response to 7.5 mM KCl and are presented as the percent KCl response. (C) EtBr uptake induced by Bz-ATP is shown for full-length and Δ-C variants. The data shown are representative of at least six independent experiments.

equivalent activity at the full-length and Δ-C variants (155 and 228 μM, respectively) (Table 1, Fig. 7A). In addition, both variants are equally sensitive to inhibition by KN-62 (68 nM full-length, 63 nM Δ-C) (Table 1, Fig. 7B) and Astra-8h (45 nM full-length, 37 nM Δ-C) (Table 1, Fig. 7C) two small molecule inhibitors. KN-62 is an isoquinolone previously demonstrated to inhibit $P2X_7$ function [21,22]. Astra-8h is a recently disclosed small molecule inhibitor of $P2X_7$ developed by Astra-Zeneca [23].

Table 1
Agonist $EC_{50}$ and antagonist $IC_{50}$ values were determined in FLIPR-based assays

| | Bz-ATP $EC_{50}$ (μM) | Ox-ATP $IC_{50}$ (μM) | KN-62 $IC_{50}$ (nM) | Astra-8h (nM) |
|---|---|---|---|---|
| Full-length | 8 ± 2 | 155 ± 48 | 68 ± 18 | 45 ± 14 |
| Δ-C | 37 ± 8 | 228 ± 78 | 63 ± 24 | 37 ± 19 |

Agonist $EC_{50}$s were determined from full dose responses. Antagonist $IC_{50}$ values were determined from antagonist dose responses tested against 30 μM Bz-ATP for full-length and 150 μM Bz-ATP for Δ-C. Values are means ± SEM for at least six independent determinations.

### *Functional analysis of $P2X_7$ variants: caspase activation*

An additional consequence of $P2X_7$ activation is the induction of proapoptotic mechanisms including activation of various caspases [5,6,24–26]. Fig. 8A shows a comparison of the Bz-ATP-induced accumulation of the neo-epitope of cytokeratin-18 which is indicative of caspase activation and triggering of the apoptotic response [27]. Bz-ATP causes an increase in accumulation of the cytokeratin neo-epitope in the full-length variant beginning at 125 μM. The response is blunted for the Δ-C variant with only the highest dose tested (1000 μM) resulting in neo-epitope accumulation. No evidence of cleavage of cytokeratin-18 was detected in the Δ-TMI cells (data not shown).

To confirm that the accumulation of the cytokeratin-18 neo-epitope was correlated with the induction of caspases, the activation of caspases 3 and 7 was examined. Bz-ATP induces an increase in caspase 3/7 activity in both full-length and Δ-C $P2X_7$ variants (Fig. 8B). No induction of caspase activity was detected in the Δ-TMI expressing cells (data not shown). Consistent with the cytokeratin cleavage analysis caspase activation was much poorer in the Δ-C variant and required higher concentrations of agonist. These data suggest that the C-terminal region of $P2X_7$ plays a role in the activation of caspases and induction of apoptosis.

## Discussion

Eight variants of the human $P2X_7$ channel were identified and isolated. These include the previously identified full-length form [28] and seven other previously unidentified splice variants. It should be noted that a BLAST search against the GenBank database reveals

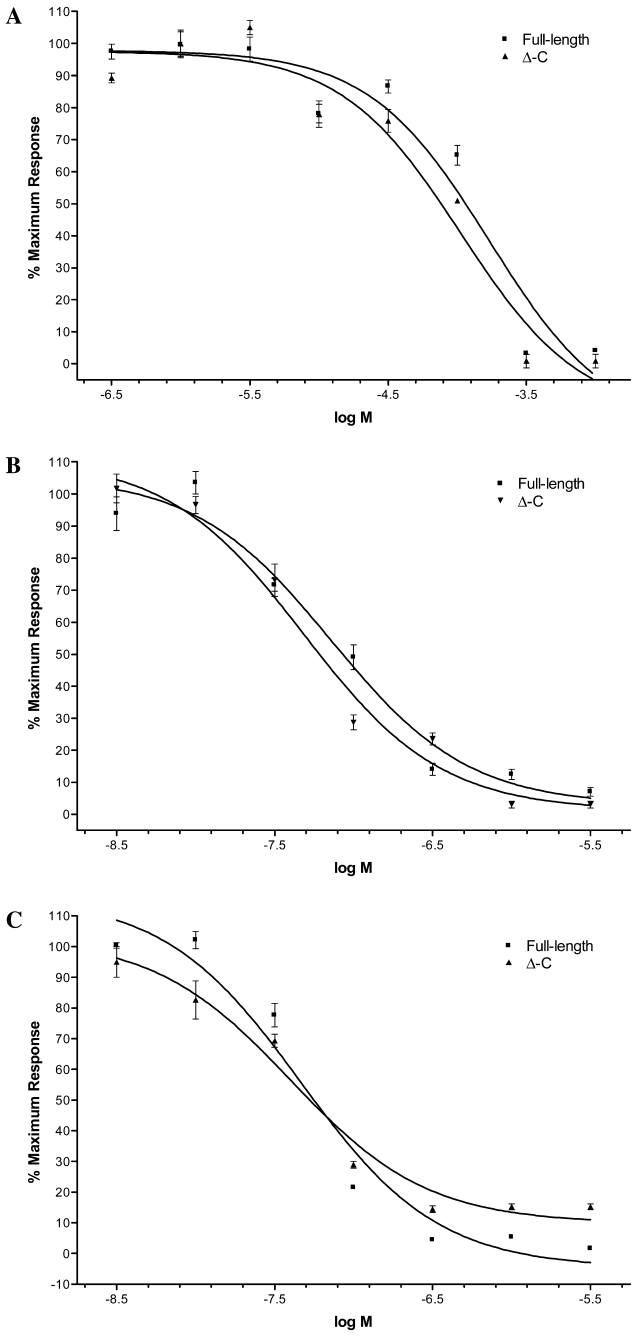


Fig. 7. Inhibition of Bz-ATP-induced $Ca^{2+}$ flux by $P2X_7$ antagonists. Inhibition curves for (A) Ox-ATP, (B) KN-62, and (C) Astra-8h are shown for full-length and Δ-C variants. Compounds were tested against 30 or 150 μM Bz-ATP, respectively, for full-length and Δ-C. The data shown are representative of at least six independent experiments.

a sequence identical to that of $P2X_7$ variant D (Accession No. NM_177427). Furthermore, another sequence (Accession No. AK090886) which is not identical to any of the variants reported here was also identified. This sequence lacks exon 2 and N3, and retains intron 10. Therefore, this sequence is the ninth variant of $P2X_7$ and can be designated variant I.

Alternative splicing has been previously described for other members of the P2X channel family. A splice variant of $P2X_1$ has been detected in human bladder by RT-PCR analysis which lacks part of the second transmembrane domain [29]. Several splice variants of the human $P2X_2$ receptor have also been identified [30]. One of these variants has a deletion within the carboxy terminus; however, this does not result in any detectable functional alterations. These findings differ from those for the rat $P2X_2$ channel in which the same alternative splicing event leads to an alteration in the desensitization of the channel [31]. Additionally, a splice variant has been identified for the human $P2X_4$ channel [32]. This variant contains a replacement of the amino terminal 90 amino acids and lacks channel function. This differs from the murine $P2X_4$ in which there is a splice variant lacking a 27 amino acid region of the extracellular portion of the receptor [33]. This variant is a poor channel but is able to form heteromeric assemblies with the full-length murine $P2X_4$ resulting in reduced affinity for ATP [33].

The variations in splicing patterns identified for $P2X_7$ in this report lead to either the inclusion of a new exon (termed N3) or the exclusion of one or more of the other 13 exons. Of most interest is the variant in which the intron between exons 10 and 11 is not excised from the final transcript. This insertion leads to the introduction of a premature stop codon truncating the last 171 amino acids of the full-length form (Fig. 3). In addition, this insertion introduces 18 new amino acids to the carboxy terminus of the Δ-C variant.

Truncation of the carboxy terminus and/or the addition of these 18 amino acids have moderate effect on the channel activity as evidenced by $Ca^{2+}$ flux and membrane potential assays. The changes in the Δ-C variant lead to a ~5-fold decrease in the potency of Bz-ATP (Table 1). Less of an effect was seen on the potency of antagonists between the two variants (Table 1). These data suggest that either an intact carboxy terminus is needed for full-agonist function or that structural changes affected by deletion of the carboxy terminus alter agonist potency. The data regarding cation channel function indicate that there are no gross differences between these forms; however, channel function has only been assessed in this report by FLIPR-based assays. More subtle differences between the full-length and Δ-C variants could exist and may require electrophysiological studies of channel activity.

The removal of the carboxy terminus has a much more profound effect on the functions of $P2X_7$ that lie downstream of the initial cation channel activity. The ability to mediate the non-specific uptake of large cationic substances such as EtBr is nearly abrogated in the Δ-C variant as is the induction of proapoptotic mechanisms such as caspase activation.

These data are consistent with mutagenesis studies in rat $P2X_7$ that have demonstrated an important role for

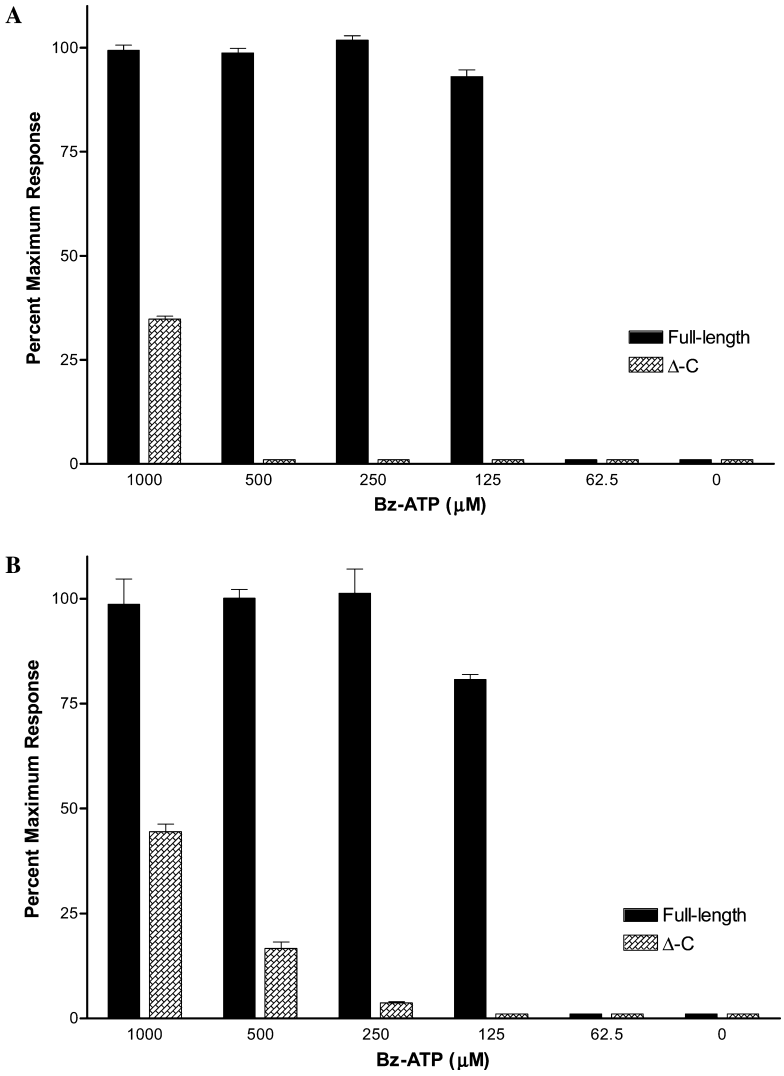


Fig. 8. Induction of proapoptotic mechanisms via $P2X_7$ variants is shown. (A) Bz-ATP-induced formation of the M30 neo-epitope of cytokeratin is shown for the full-length and Δ-C variants. (B) Bz-ATP-induced caspase 3 and 7 activation is shown for the full-length and Δ-C variants. The data shown are representative of at least three independent experiments.

the carboxy terminus in $P2X_7$ function [4]. Other studies on human $P2X_7$ have identified a naturally occurring polymorphism that leads to a single amino acid substitution in the carboxy terminal region of the protein [34]. This mutation results in the inability to trigger pore formation and apoptotic mechanisms [34] similar to the Δ-C splice variant. In addition, it has been shown that the electrophysiological properties of this polymorph are not altered [35] similar to our findings with the Δ-C variant.

It appears from these and other data that the carboxy terminus of $P2X_7$ is dispensable for the initial cation channel activity triggered by ATP. However, further downstream events appear to require the presence of this domain. Indeed, this region has been suggested to contain protein interaction domains and has been shown to contain a region that is capable of binding lipopolysaccharide (LPS) [36]. Another recent study suggests the existence of a $P2X_7$ signaling complex [37]. Proteomic analysis was used to show the interaction of $P2X_7$ with multiple proteins including laminin α3, integrin β2, β-actin, α-actinin, supervillin, MAGuK, three heat shock proteins, phosphatidylinositol 4-kinase, and receptor protein tyrosine phosphatase-β. Although the specific region of $P2X_7$ involved in these interactions was not elucidated, it is speculated that several of the cytoskeletal and other intracellular proteins would interact with the carboxy terminus of $P2X_7$. In addition, Kim et al. showed that activation of $P2X_7$ leads to the dephosphorylation of the channel at Tyr 343. This activation-dependent dephosphorylation appears to be necessary for the current run-down seen after repeated short applications of agonist to the channel but not for the initial current. The total current through the channel is normally decreased by repeated agonist additions. In the presence of phosphatase inhibitors or in a

Y343F $P2X_7$ mutant, the current run-down is ablated and repeated applications of agonist result in a consistently high current. It is noteworthy that this residue (Y343) is maintained in the Δ-C splice variant, suggesting that important elements for cation channel function are maintained.

Another surprising finding from the current study is that the Δ-C splice variant appears to be the predominant $P2X_7$ transcript in many tissues. It is unclear whether this means that the Δ-C form of the protein is indeed the predominant form expressed; however, it is clear from the recombinant studies that this variant can be effectively expressed and maintains channel function. The implications of this are unknown. These data suggest that there may be many tissue and cell types that express $P2X_7$ which would not be subjected to the downstream apoptotic and pore formation functions of the channel.

The ATP-mediated processing of pro-IL-1β to the mature form by caspase-1 is an important function of $P2X_7$. It is suggested that the activation of caspase-1 is a result of the efflux of $K^+$ that is facilitated by $P2X_7$ activation [14,38–40]. While it has not been directly tested in this report, it is reasonable to speculate that this function of $P2X_7$ would remain intact for the Δ-C variant. The FLIPR data generated herein suggest that channel activity is not grossly disrupted in this variant; however, more subtle effects cannot be ruled out. The fact that induction of caspase 3/7 activity is inhibited in the Δ-C variant suggests that this process does not simply require intact channel activity but relies on elements within the carboxy terminus. Thus, activation of proapoptotic caspases may be effected through a different mechanism than that responsible for activation of ICE.

The active $P2X_7$ channel is likely a homotrimer [1]. Still to be elucidated is whether the Δ-C variant and full-length forms of the protein are able to interact to form heteromultimeric channels. The functional implication for this is also unknown but it is interesting to speculate that controlling the expression level of the Δ-C splice variant may yield very subtle control over the various functions of $P2X_7$ within different tissues and cells.

## References


[1] R.A. North, Molecular physiology of P2X receptors, Physiol. Rev. 82 (2002) 1013–1067.

[2] R.A. North, A. Surprenant, Pharmacology of cloned P2X receptors, Annu. Rev. Pharmacol. Toxicol. 40 (2000) 563–580.

[3] C. Virginio, A. MacKenzie, R.A. North, A. Surprenant, Kinetics of cell lysis, dye uptake and permeability changes in cells expressing the rat P2X7 receptor, J. Physiol. 519 (Pt. 2) (1999) 335–346.

[4] A. Surprenant, F. Rassendren, E. Kawashima, R.A. North, G. Buell, The cytolytic P2Z receptor for extracellular ATP identified as a P2X receptor (P2X7), Science 272 (1996) 735–738.

[5] R. Coutinho-Silva, P.M. Persechini, R.D. Bisaggio, J.L. Perfettini, A.C. Neto, J.M. Kanellopoulos, I. Motta-Ly, A. Dautry-Varsat, D.M. Ojcius, P2Z/P2X7 receptor-dependent apoptosis of dendritic cells, Am. J. Physiol. 276 (1999) C1139–C1147.

[6] D. Ferrari, M. Los, M.K. Bauer, P. Vandenabeele, S. Wesselborg, K. Schulze-Osthoff, P2Z purinoreceptor ligation induces activation of caspases with distinct roles in apoptotic and necrotic alterations of cell death, FEBS Lett. 447 (1999) 71–75.

[7] D. Ferrari, P. Chiozzi, S. Falzoni, M. Dal Susino, L. Melchiorri, O.R. Baricordi, F. Di Virgilio, Extracellular ATP triggers IL-1 beta release by activating the purinergic P2Z receptor of human macrophages, J. Immunol. 159 (1997) 1451–1458.

[8] D. Ferrari, P. Chiozzi, S. Falzoni, S. Hanau, F. Di Virgilio, Purinergic modulation of interleukin-1 beta release from microglial cells stimulated with bacterial endotoxin, J. Exp. Med. 185 (1997) 579–582.

[9] R.E. Laliberte, D.G. Perregaux, P. McNiff, C.A. Gabel, Human monocyte ATP-induced IL-1 beta posttranslational processing is a dynamic process dependent on in vitro growth conditions, J. Leukoc. Biol. 62 (1997) 227–239.

[10] D.G. Perregaux, R.E. Laliberte, C.A. Gabel, Human monocyte interleukin-1beta posttranslational processing. Evidence of a volume-regulated response, J. Biol. Chem. 271 (1996) 29830–29838.

[11] D.G. Perregaux, C.A. Gabel, Human monocyte stimulus-coupled IL-1beta posttranslational processing: modulation via monovalent cations, Am. J. Physiol. 275 (1998) C1538–C1547.

[12] R. Coutinho-Silva, J.L. Perfettini, P.M. Persechini, A. Dautry-Varsat, D.M. Ojcius, Modulation of P2Z/P2X(7) receptor activity in macrophages infected with *Chlamydia psittaci*, Am. J. Physiol. Cell Physiol. 280 (2001) C81–C89.

[13] D.J. Kusner, J. Adams, ATP-induced killing of virulent *Mycobacterium tuberculosis* within human macrophages requires phospholipase D, J. Immunol. 164 (2000) 379–388.

[14] J.M. Kahlenberg, G.R. Dubyak, Mechanisms of caspase-1 activation by P2X7 receptor-mediated $K^+$ release, Am. J. Physiol. Cell Physiol. (2003).

[15] L. Gudipaty, J. Munetz, P.A. Verhoef, G.R. Dubyak, Essential role for $Ca^{2+}$ in regulation of IL-1beta secretion by P2X7 nucleotide receptor in monocytes, macrophages, and HEK-293 cells, Am. J. Physiol. Cell Physiol. 285 (2003) C286–C299.

[16] M. Solle, J. Labasi, D.G. Perregaux, E. Stam, N. Petrushova, B.H. Koller, R.J. Griffiths, C.A. Gabel, Altered cytokine production in mice lacking P2X(7) receptors, J. Biol. Chem. 276 (2001) 125–132.

[17] J.M. Labasi, N. Petrushova, C. Donovan, S. McCurdy, P. Lira, M.M. Payette, W. Brissette, J.R. Wicks, L. Audoly, C.A. Gabel, Absence of the P2X7 receptor alters leukocyte function and attenuates an inflammatory response, J. Immunol. 168 (2002) 6436–6445.

[18] A.D. Michel, R. Kaur, I.P. Chessell, P.P. Humphrey, Antagonist effects on human P2X(7) receptor-mediated cellular accumulation of YO-PRO-1, Br. J. Pharmacol. 130 (2000) 513–520.

[19] G.N. Buell, F. Talabot, A. Gos, J. Lorenz, E. Lai, M.A. Morris, S.E. Antonarakis, Gene structure and chromosomal localization of the human P2X7 receptor, Receptors Channels 5 (1998) 347–354.

[20] J.S. Wiley, R. Chen, G.P. Jamieson, The ATP4− receptor-operated channel (P2Z class) of human lymphocytes allows $Ba^{2+}$ and ethidium+ uptake: inhibition of fluxes by suramin, Arch. Biochem. Biophys. 305 (1993) 54–60.

[21] C.E. Gargett, J.S. Wiley, The isoquinoline derivative KN-62 a potent antagonist of the P2Z-receptor of human lymphocytes, Br. J. Pharmacol. 120 (1997) 1483–1490.

[22] P.G. Baraldi, M. del Carmen Nunez, A. Morelli, S. Falzoni, F. Di Virgilio, R. Romagnoli, Synthesis and biological activity of N-arylpiperazine-modified analogues of KN-62, a potent antagonist of the purinergic P2X7 receptor, J. Med. Chem. 46 (2003) 1318–1329.

[23] L. Alcaraz, A. Baxter, J. Bent, K. Bowers, M. Braddock, D. Cladingboel, D. Donald, M. Fagura, M. Furber, C. Laurent, M. Lawson, M. Mortimore, M. McCormick, N. Roberts, M. Robertson, Novel P2X7 receptor antagonists, Bioorg. Med. Chem. Lett. 13 (2003) 4043–4046.
[24] C. Goepfert, M. Imai, S. Brouard, E. Csizmadia, E. Kaczmarek, S.C. Robson, CD39 modulates endothelial cell activation and apoptosis, Mol. Med. 6 (2000) 591–603.
[25] E. Schulze-Lohoff, C. Hugo, S. Rost, S. Arnold, A. Gruber, B. Brune, R.B. Sterzel, Extracellular ATP causes apoptosis and necrosis of cultured mesangial cells via P2Z/P2X7 receptors, Am. J. Physiol. 275 (1998) F962–F971.
[26] S.C. Chow, G.E. Kass, S. Orrenius, Purines and their roles in apoptosis, Neuropharmacology 36 (1997) 1149–1156.
[27] M.P. Leers, W. Kolgen, V. Bjorklund, T. Bergman, G. Tribbick, B. Persson, P. Bjorklund, F.C. Ramaekers, B. Bjorklund, M. Nap, H. Jornvall, B. Schutte, Immunocytochemical detection and mapping of a cytokeratin 18 neo-epitope exposed during early apoptosis, J. Pathol. 187 (1999) 567–572.
[28] F. Rassendren, G.N. Buell, C. Virginio, G. Collo, R.A. North, A. Surprenant, The permeabilizing ATP receptor, P2X7. Cloning and expression of a human cDNA, J. Biol. Chem. 272 (1997) 5482–5486.
[29] L.A. Hardy, I.J. Harvey, P. Chambers, J.I. Gillespie, A putative alternatively spliced variant of the P2X(1) purinoreceptor in human bladder, Exp. Physiol. 85 (2000) 461–463.
[30] K.J. Lynch, E. Touma, W. Niforatos, K.L. Kage, E.C. Burgard, T. van Biesen, E.A. Kowaluk, M.F. Jarvis, Molecular and functional characterization of human P2X(2) receptors, Mol. Pharmacol. 56 (1999) 1171–1181.
[31] U. Brandle, P. Spielmanns, R. Osteroth, J. Sim, A. Surprenant, G. Buell, J.P. Ruppersberg, P.K. Plinkert, H.P. Zenner, E. Glowatzki, Desensitization of the P2X(2) receptor controlled by alternative splicing, FEBS Lett. 404 (1997) 294–298.
[32] P.D. Dhulipala, Y.X. Wang, M.I. Kotlikoff, The human P2X4 receptor gene is alternatively spliced, Gene 207 (1998) 259–266.
[33] A. Townsend-Nicholson, B.F. King, S.S. Wildman, G. Burnstock, P.D. Dhulipala, Y.X. Wang, M.I. Kotlikoff, Molecular cloning, functional characterization and possible cooperativity between the murine P2X4 and P2X4a receptors, Brain Res. Mol. Brain Res. 64 (1999) 246–254.
[34] B.J. Gu, W. Zhang, R.A. Worthington, R. Sluyter, P. Dao-Ung, S. Petrou, J.A. Barden, J.S. Wiley, A Glu-496 to Ala polymorphism leads to loss of function of the human P2X7 receptor, J. Biol. Chem. 276 (2001) 11135–11142.
[35] W. Boldt, M. Klapperstuck, C. Buttner, S. Sadtler, G. Schmalzing, F. Markwardt, Glu496Ala polymorphism of human P2X7 receptor does not affect its electrophysiological phenotype, Am. J. Physiol. Cell Physiol. 284 (2003) C749–C756.
[36] L.C. Denlinger, P.L. Fisette, J.A. Sommer, J.J. Watters, U. Prabhu, G.R. Dubyak, R.A. Proctor, P.J. Bertics, Cutting edge: the nucleotide receptor P2X7 contains multiple protein- and lipid-interaction motifs including a potential binding site for bacterial lipopolysaccharide, J. Immunol. 167 (2001) 1871–1876.
[37] M. Kim, L.H. Jiang, H.L. Wilson, R.A. North, A. Surprenant, Proteomic and functional evidence for a P2X7 receptor signalling complex, EMBO J. 20 (2001) 6347–6358.
[38] D. Perregaux, J. Barberia, A.J. Lanzetti, K.F. Geoghegan, T.J. Carty, C.A. Gabel, IL-1 beta maturation: evidence that mature cytokine formation can be induced specifically by nigericin, J. Immunol. 149 (1992) 1294–1303.
[39] D. Perregaux, C.A. Gabel, Interleukin-1 beta maturation and release in response to ATP and nigericin. Evidence that potassium depletion mediated by these agents is a necessary and common feature of their activity, J. Biol. Chem. 269 (1994) 15195–15203.
[40] I. Walev, K. Reske, M. Palmer, A. Valeva, S. Bhakdi, Potassium-inhibited processing of IL-1 beta in human monocytes, EMBO J. 14 (1995) 1607–1614.